World Journal of Gastroenterology

Online Submissions: http://www.wjgnet.com/esps/
bpgoffice@wjgnet.com
doi:10.3748/wjg.v19.i47.9092

World J Gastroenterol 2013 December 21; 19(47): 9092-9103
ISSN 1007-9327 (print) ISSN 2219-2840 (online)

BRIEF ARTICLE

Separate calculation of DW-MRI in assessing therapeutic effect in liver tumors in rats

Feng Chen, Frederik De Keyzer, Yuan-Bo Feng, Marlein Miranda Cona, Jie Yu, Guy Marchal, Raymond Oyen, Yi-Cheng Ni

Feng Chen, Department of Radiology, the First Affiliated Hospital, College of Medicine, Zhejiang University, Hangzhou 310003, Zhejiang Province, China

Feng Chen, Frederik De Keyzer, Yuan-Bo Feng, Marlein Miranda Cona, Jie Yu, Guy Marchal, Raymond Oyen, Yi-Cheng Ni, Theragnostic Laboratory, Department of Imaging and Pathology, University Hospital, University of Leuven, Herestraat 49, Bus 7003, 3000 Leuven, Belgium

Author contributions: All the authors substantially contributed to conception and design, acquisition of data, or analysis and interpretation of data, drafting the article or revising it critically for important intellectual content, and final approval of the version to be published; Chen F, Feng YB, Yu J and Ni YC conducted animal experiments; Chen F and Keyzer FD performed statistical analyses.

Supported by National Natural Science Foundation of China, No. 30670603

Correspondence to: Feng Chen, MD, PhD, Deputy Director, Department of Radiology, the First Affiliated Hospital, College of Medicine, Zhejiang University, 79 Qingchun Road, Hangzhou 310003, Zhejiang Province, China. chenfengbe@aliyun.com
Telephone: +86-571-87236587 Fax: +86-571-87236587

Received: July 31, 2013 Revised: October 19, 2013
Accepted: November 3, 2013
Published online: December 21, 2013

Abstract

AIM: To explore whether the antitumor effect of a vascular disrupting agent (VDA) would be enhanced by combining with an antiangiogenic agent, and whether such synergistic effects can be effectively evaluated with separate calculation of diffusion weighted magnetic resonance imaging (DW-MRI).

METHODS: Thirty-seven rats with implanted liver tumors were randomized into the following three groups: (1) ZD6126, a kind of VDA; (2) ZDTHA, ZD6126 in combination with an antiangiogenic, thalidomide; and (3) control. Morphological DW-MRI were performed and quantified before, 4 h and 2 d after treatment. The apparent diffusion coefficient (ADC) values were calculated separately for low *b* values (ADC_{low}), high *b* values (ADC_{high}) and all *b* values (ADC_{all}). The tissue perfusion contribution, ADC_{perf}, was calculated as ADC_{low}-ADC_{high}. Imaging findings were finally verified by histopathology.

RESULTS: The combination therapy with ZDTHA significantly delayed tumor growth due to synergistic effects by inducing cumulative tumor necrosis. In addition to delaying tumor growth, ZDTHA caused tumor necrosis in an additive manner, which was verified by HE staining. Although both ADC_{high} and ADC_{all} in the ZD6126 and ZDTHA groups were significantly higher compared to those in the control group on day 2, the entire tumor ADC_{high} of ZDTHA was even higher than that of ZD6126, but the significant difference was not observed for ADC_{all} between ZDTHA and ZD6126. This indicated that the perfusion insensitive ADC_{high} values calculated from high *b* value images performed significantly better than ADC_{all} for the monitoring of tumor necrosis on day 2. The perfusion sensitive ADC_{perf} derived from ADC_{low} by excluding high *b* value effects could better reflect the reduction of blood flow due to the vessel shutdown induced by ZD6126, compared to the ADC_{low} at 4 h. The ADC_{perf} could provide valuable perfusion information from DW-MRI data.

CONCLUSION: The separate calculation of ADC is more useful than conventional averaged ADC in evaluating the efficacy of combination therapy with ZD6126 and thalidomide for solid tumors.

Key words: Diffusion weighted imaging; Magnetic resonance imaging; Therapeutic assessment; Liver tumor; Rats; Vascular disrupting agent; Antiangiogenic agent;

Animal model; Rodents

Core tip: The combination therapy with ZD6126 and thalidomide significantly delayed liver tumor growth due to synergistic effects by inducing cumulative tumor necrosis in rodents. The apparent diffusion coefficient $(ADC)_{high}$ performed significantly better than ADC_{all} for the monitoring of tumor necrosis on day 2. The ADC_{perf} could better reflect the reduction of blood flow due to the vessel shutdown induced by ZD6126, compared to the ADC_{low}. The ADC_{perf} could provide valuable perfusion information from diffusion weighted magnetic resonance imaging data.

Chen F, Keyzer FD, Feng YB, Cona MM, Yu J, Marchal G, Oyen R, Ni YC. Separate calculation of DW-MRI in assessing therapeutic effect in liver tumors in rats. *World J Gastroenterol* 2013; 19(47): 9092-9103 Available from: URL: http://www.wjgnet.com/1007-9327/full/v19/i47/9092.htm DOI: http://dx.doi.org/10.3748/wjg.v19.i47.9092

INTRODUCTION

Tumor vasculature has become an attractive target for therapy. One of such therapies is to use vascular disrupting agents (VDAs), which can selectively destroy existing tumor blood vessels by disrupting the microtubules of the cytoskeleton in endothelial cells; this leads to ischemic central necrosis of the tumor[1]. However, tumors can rapidly rebound from the residual viable rim when VDAs are used alone; this compromises the therapeutic utility of these agents[2]. Another therapy is to prevent new tumor blood vessel formation with antiangiogenic agents. Therefore, current efforts have gradually shifted from the single use of VDA to the combination of a VDA with an antiangiogenic agent[3,4]. As the latter may inhibit the growth of new tumor vessels, the combination of two approaches thus is likely to have synergistic therapeutic efficacy.

As an established non-invasive technique, *in vivo* magnetic resonance imaging (MRI) has played an important role in the evaluation of tumor response to treatment. Diffusion-weighted MRI (DW-MRI), due to its ability to detect molecular water motion at the cellular level, *i.e.*, the measurement of tissue apparent diffusion coefficient (ADC), has become a favorite choice of measures in a variety of oncological studies and tissue viability assessments[5]. Technological innovations in recent years have enabled the increasing use of high-quality and quantitative DW-MRI in monitoring tumor treatment. However, it has been realized that the information acquired from conventional calculation of DW-MRI data actually represents the combined effects of tissue microcirculation perfusion and pure tissue diffusivity in each imaging voxel at DW-MRI. This may hinder the appropriate interpretation of the DW-MRI data[6]. Therefore, there is growing interest in applying more sophisticated approaches, such as separate ADC (calculating different ADC values based on various combinations of *b* values with a monoexponential fitting algorithm)[7-9] and intravoxel incoherent motion (IVIM)[10,11], to differentiate the fraction of microcirculation perfusion from pure diffusivity within the DW-MRI data.

The purpose of the present study was to test our hypotheses that the antitumor effect of a VDA, ZD6126, would be enhanced by combining with an antiangiogenic agent, thalidomide, and that the effect can be monitored and better elucidated with separate calculation of ADC values compared to conventional ADC value in a rat liver tumor model. To our knowledge, the application of separate calculation of ADC maps has not been reported in such a combined antitumor therapy.

MATERIALS AND METHODS

Experimental design

A total of 37 rats were randomly assigned into the following 3 groups: (1) ZD6126 group (n = 14): ZD6126 (AstraZeneca, Cheshire, United Kingdom) was dissolved with 4 portions of 8.4% sodium carbonate and 1 portion of phosphate-buffered saline (PBS), pH 7.4. On day 0, one dose of 50 mg/kg ZD6126 was injected *iv* into each animal; (2) ZDTHA group (n = 13): Stock solutions of thalidomide (Pharmaceutical Factory, Changzhou, China) were prepared in DMSO (Sigma-Aldrich NV/SA, Bornem, Belgium) and injected *ip* at a dose of 200 mg/kg three times at a interval of one day during the entire experiment[12]; the first dose of thalidomide was injected 24 h prior to ZD6126 administration, and the second and third doses of thalidomide were given immediately and 2 d after ZD6126 administration, respectively; and (3) Control group (n = 10): Animals were *iv* and *ip* injected with the vehicles (solvents) of both agents at the same time points that the other groups were injected. For all groups, MRI was performed before, and 4 h and 2 d after the initial ZD6126 treatment. At the end of the experiment, all animals were sacrificed for histopathological examinations.

Animal model

This study was approved by the institutional ethical committee for the use and care of laboratory animals. Adult WAG/Rij rats (Iffa Credo, Brussels, Belgium) with existing subcutaneous rhabdomyosarcomas were used as donors. The tumor tissues were excised and implanted into 37 normal adult WAG/Rij rats that weighed 225-275 g, as described previously[13].

MRI

All rats were initially anesthetized by inhalation of 2% isoflurane and maintained with 0.8% isoflurane for MRI. A clinical 1.5T MRI system (Sonata, Siemens, Erlangen, Germany) was used with a maximum gradient capability of 40 mT/m. The following sequences were acquired in the transverse plane for all rats, with a slice thickness of 2 mm and an inter-slice gap of 0.2 mm: (1) Fat saturated

T2-weighted fast spin echo MRI (T2W-MRI) with a repetition/echo time (TR/TE) of 3860/106 ms, a turbo factor of 19, a field of view (FOV) of 140 mm × 70 mm, and an acquisition matrix of 256 × 256 (in-plane resolution: 0.5 mm × 0.3 mm). Three signals were acquired, in a scan time of 1 min 25 s; (2) Contrast-enhanced fat saturated T1-weighted fast spin echo MRI (CE-T1W-MRI) immediately after an *iv* bolus of 0.3 mmol/kg gadoterate meglumine (Dotarem®, Guerbet, France), with the following parameters: a TR/TE of 535/9.2 ms, a turbo factor of seven, a FOV of 140 mm × 70 mm, and an acquisition matrix of 256 × 256 (in-plane resolution: 0.5 mm × 0.3 mm). Four signals were acquired, in a scan time of 1 min 24 s; (3) DW-MRI with a 2-dimensional (2D), spin echo, echo-planar imaging sequence. We used a TR/TE of 1700/83 ms, a FOV of 140 mm × 82 mm, and an acquisition matrix of 192 × 91 (in-plane resolution: 0.7 mm × 0.9 mm). For the DW-MRI, six signals were acquired, including repeated measurements for 10 different *b* values (0, 50, 100, 150, 200, 250, 300, 500, 750, and 1000 s/mm^2) in 3 directions (*x*, *y*, and *z*) and averaged for the calculation of the isotropic ADC value. A parallel imaging technique was applied to reduce susceptibility artifacts and examination times. The total examination time was 4 min 51 s.

Tissue processing and histology

All rats were euthanized for tissue processing and histology at the end of the experiment. First, animals were over-anesthetized by an intraperitoneal injection of pentobarbital (50 mg/kg) (Nembutal, Sanofi Sante Animale, Brussels, Belgium). Then, the livers were collected, fixed with formalin, embedded in paraffin, and sliced into transverse sections. The sections were 2 mm thick, and were positioned on the same planes used for the MRI scans, based on a grid (Agar Scientific, England). The tumor slices (5 μm thick) were stained with hematoxylin and eosin (HE).

MRI analysis

An off-line LINUX workstation with dedicated software (Biomap, Novartis, Basel, Switzerland) was used for image analyses. Two experienced radiologists delineated the entire tumor with operator-defined regions of interest (ROI) in consensus to obtain robust measurements and to facilitate comparisons between different treatment approaches. All ROIs were larger than 10 pixels in size. For each imaging parameter, tumor and normal liver were measured with ROIs on all tumor-containing image slices, and mean values were obtained for each tumor and the liver, respectively. After that, the mean value and standard deviation for each parameter were calculated for each group at each time point for statistical analysis.

T2 weighted and contrast enhanced-T1 weighted MRI: The residual viable tumor or rim after treatment was visualized as contrast-enhanced, high signal region on the CE-T1W-MRI. The tumor necrotic areas were contoured on CE-T1W-MRI based on the unenhanced, low-signal areas within the tumors that were observed after injection of a contrast agent. Relative volumes (%) of tumor necrosis were calculated by normalizing them to the entire tumor volume. For each lesion, the tumor areas were delineated at T2W-MRI on all slices and automatically combined into the total tumor volume. The tumor volume change (%) was calculated using the following formula: [(volume$_{post}$ - volume$_{pre}$)/volume$_{pre}$] × 100.

Separate calculation of tumor ADC: For calculating different ADC values, the first step was to measure the entire tumor signal intensity (SI) from original DW-MRI images of 10 *b* values, respectively. Briefly, for each tumor, freehand delineations were performed on all slices of the original DW-MRI at a *b* value of 1000 s/mm^2. These delineations were merged to form one 3D volume of interest per lesion. The volume of interest was then automatically copied to all images with different *b* values and the average SI of each lesion per *b* value was determined. The second step was to obtain separate ADC values according to a monoexponential model using all 10 *b* values[14]. To differentiate the individual contributions of tissue microcapillary perfusion and pure tissue diffusivity, the ADC values of each tumor were obtained separately for low *b* values (*b* = 0, 50, and 100 s/mm^2; ADC$_{low}$) and high *b* values (*b* = 500, 750, and 1000 s/mm^2; ADC$_{high}$) from the average SI per tumor and per *b* value. Each ADC value was calculated by using a least squares solution of the following system of equations: ADC$_{all}$: $S_k = S_0 \times exp(-b_k \times ADC_{low})$, for k = 0, 50, 100; 150, 200, 250, 300, 500, 750, 1000; ADC$_{low}$: $S_i = S_0 \times exp(-b_i \times ADC_{low})$, for i = 0, 50, 100; ADC$_{high}$: $S_j = S_0 \times exp(-b_j \times ADC_{high})$, for j = 500, 750, 1000; where S_k, S_i, and S_j are the SI measured on the DW-MRI acquired with the corresponding *b* values b_k, b_i and b_j, S_0 represents the exact SI (without the influence of noise induced by the MR measurement) with *b* value equal to 0 s/mm^2. ADC$_{low}$ is perfusion sensitive, while ADC$_{high}$ is perfusion insensitive. Although ADC$_{low}$ is perfusion sensitive, it is also affected by diffusion effects in tissue[15]. Therefore, an approximate indicator, ADC$_{perf}$, for the tissue perfusion contribution can be calculated as ADC$_{low}$-ADC$_{high}$[7]. Imaging software (MeVisLab 2.2.1, MeVis Medical Solutions AG, Bremen, Germany) was used to generate the maps of ADC$_{all}$, ADC$_{high}$, ADC$_{low}$ and ADC$_{perf}$.

Microscopic analysis

Microscopic image analyses were performed by a pathologist blinded to the experimental detail with magnifications ranging from × 50 to × 400. On HE stained macroscopic sections, image analysis software (ImageJ 1.34s, NIH, United States) was used to quantify the percentages of amorphous eosinophilic necrosis in the total tumor area.

Statistical analysis

Statistical analysis was carried out with the SPSS for win-

dows software package (release 18.0, SPSS Inc., Chicago, United States). A general linear model, with repeated-measures, was used to compare changes in various parameters over time among groups. The nonparametric Kruskal-Wallis analysis of variance was performed for comparing parameters between groups at certain time points, followed by post-hoc group-wise comparisons using a Bonferroni correction for multiple tests. A P value < 0.05 was considered statistically significant.

RESULTS

A total of 37 rats (72 tumors) were included in the study. Four rats in the ZDTHA group were found to have minor hemorrhage around the eye socket and perianal area on day 1 after the first thalidomide treatment. This was probably due to a venous thromboembolism induced by thalidomide[16].

Tumor volume growth

As shown on T2W-MRI images, ZD6126 and ZDTHA both induced a significant tumor volume growth delay from pretreatment to 2 d after administration, compared to the control group ($P < 0.0001$ for both). Furthermore, ZDTHA performed significantly better than ZD6126 in delaying tumor growth on day 2 after treatment ($P < 0.0001$) (Figure 1).

Perfusion insensitive ADC_{high}: Before treatment: there were no significant differences in ADC_{high} among the three groups ($P > 0.05$ for all). At 4 h, there was no significant change in the ADC_{high} ($P > 0.05$ for both) in both the ZDTHA and ZD6126 groups, compared to the control group. On day 2, the therapy-induced tumor necrosis caused a significant rise in the ADC_{high} in both ZDTHA and ZD6126 groups compared to the control group ($P < 0.0001$ and $= 0.0004$, respectively). Furthermore, the ADC_{high} was much higher in the ZDTHA group than in the ZD6126 group ($P = 0.03$) (Table 1 and Figure 2A-C).

ADC_{all}: At 4 h, the ADC_{all} in both the ZDTHA and ZD6126 groups was significantly reduced compared to the control group ($P = 0.01$ and 0.02, respectively). In contrast, the ADC_{all} in both the ZDTHA and ZD6126 groups showed a sharp increase on day 2 compared to the control group ($P < 0.0001$ for both). However, no difference in ADC_{all} was found between the ZDTHA and ZD6126 groups ($P = 0.08$) (Table 1 and Figure 2A-C).

Comparison of ADC_{high} with ADC_{all}: The performance of ADC_{all} was different with that of ADC_{high} at the following time points. At 4 h, the ADC_{all} in both the ZDTHA and ZD6126 groups showed a significant decrease compared to the control group; however, this was not observed for ADC_{high} in the same two groups. On day 2, the ADC_{high} of ZDTHA was significantly greater than that of ZD6126 ($P = 0.03$), but the significant difference was not observed for ADC_{all} between the ZDTHA and ZD6126 groups ($P = 0.08$) (Table 1 and Figure 2A-C).

ADC_{low} and perfusion sensitive ADC_{perf}

ADC_{low}: The ADC_{low} of ZDTHA was significantly lower than that of ZD6126 before treatment ($P < 0.05$), but it was not for the control group ($P = 0.12$). No significant differences in ADC_{low} were observed among the three groups at 4 h ($P > 0.05$ for all). On day 2, the ADC_{low} of ZDTHA was much higher compared to the control group ($P = 0.02$) (Table 1 and Figure 2D-F).

ADC_{perf}: Compared to the control group, tumor ADC_{perf} in both the ZD6126 and ZDTHA groups decreased dramatically at 4 h, most likely due to a rapid vascular shutdown induced by ZD6126 ($P = 0.016$ and 0.047, respectively). This was followed by a rapid rebound on day 2 in both the ZD6126 and ZDTHA groups (no longer significantly different compared to the control group, $P = 0.979$ and 0.525, respectively) (Figure 2D-F). A significant reduction in the tumor ADC_{perf} of ZDTHA was noted at 4 h compared to the ZD6126 group ($P = 0.025$). The ADC_{perf} of ZDTHA still showed a lower level compared to the ZD6126 at 2 d, although there was no significant difference ($P = 0.44$) (Table 1 and Figure 2D-F).

Histology

Two days after treatment, the percentages of necrosis compared to the total tumor areas on HE stained tumor sections were significantly higher in both the ZDTHA and ZD6126 groups compared to the control group ($P = 0.000$ for both). No significant difference was found in the necrotic areas of the ZDTHA and ZD6126 groups ($P = 0.09$) (Figure 1).

DISCUSSION

We have demonstrated three main findings in the present study. First, tumor growth was significantly delayed by both ZD6126 and ZDTHA treatments compared to the control group, and a significant delay could be observed only two days after application of a single dose of ZD6126. In addition, ZDTHA significantly delayed tumor growth than ZD6126, indicating a synergistic anticancer effect of ZD6126 and thalidomide. It has been known that tumors can rapidly regrow due to the residual viable rim when ZD6126 was used alone[2]. It has also been reported that thalidomide, which was reintroduced into clinical practice with its antiangiogenic properties, had little or no effect on full-grown tumors like those in our patients, when used alone[4]. Therefore, the synergistic effects of ZDTHA may have contributed to the enhanced antitumor effect in this study. In the combination therapy, ZD6126-induced tumor necrosis, which may then promote tumor angiogenesis, could provide the appropriate conditions for THA to indirectly inhibit angiogenesis[17], because thalidomide is effective only in the early stages of tumor formation[4]. Thalidomide indirectly inhibits angiogenesis *via* tumor necrosis factor and

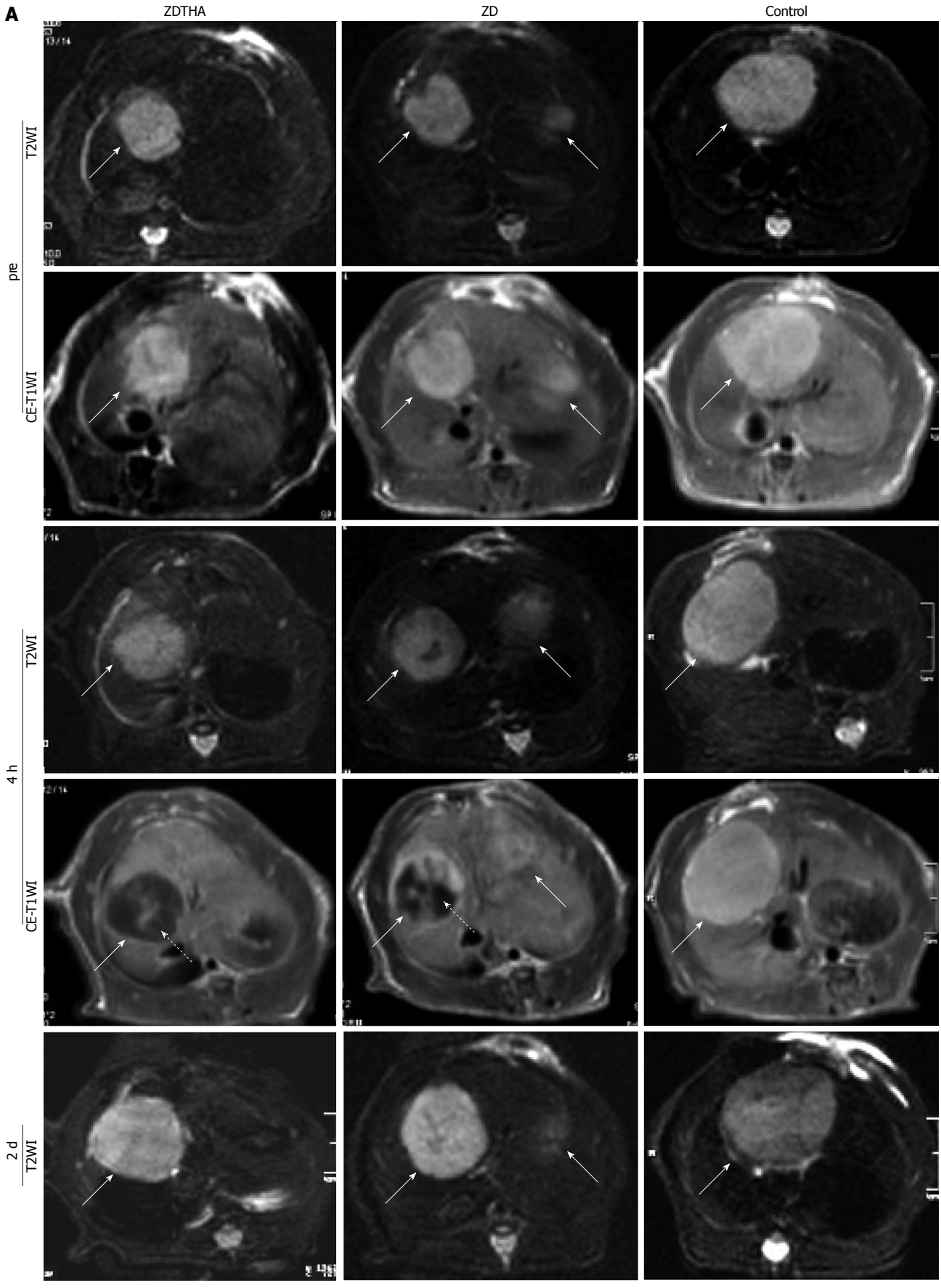
A
ZDTHA
ZD
Control
pre
T2WI
CE-T1WI
4 h
T2WI
CE-T1WI
2 d
T2WI

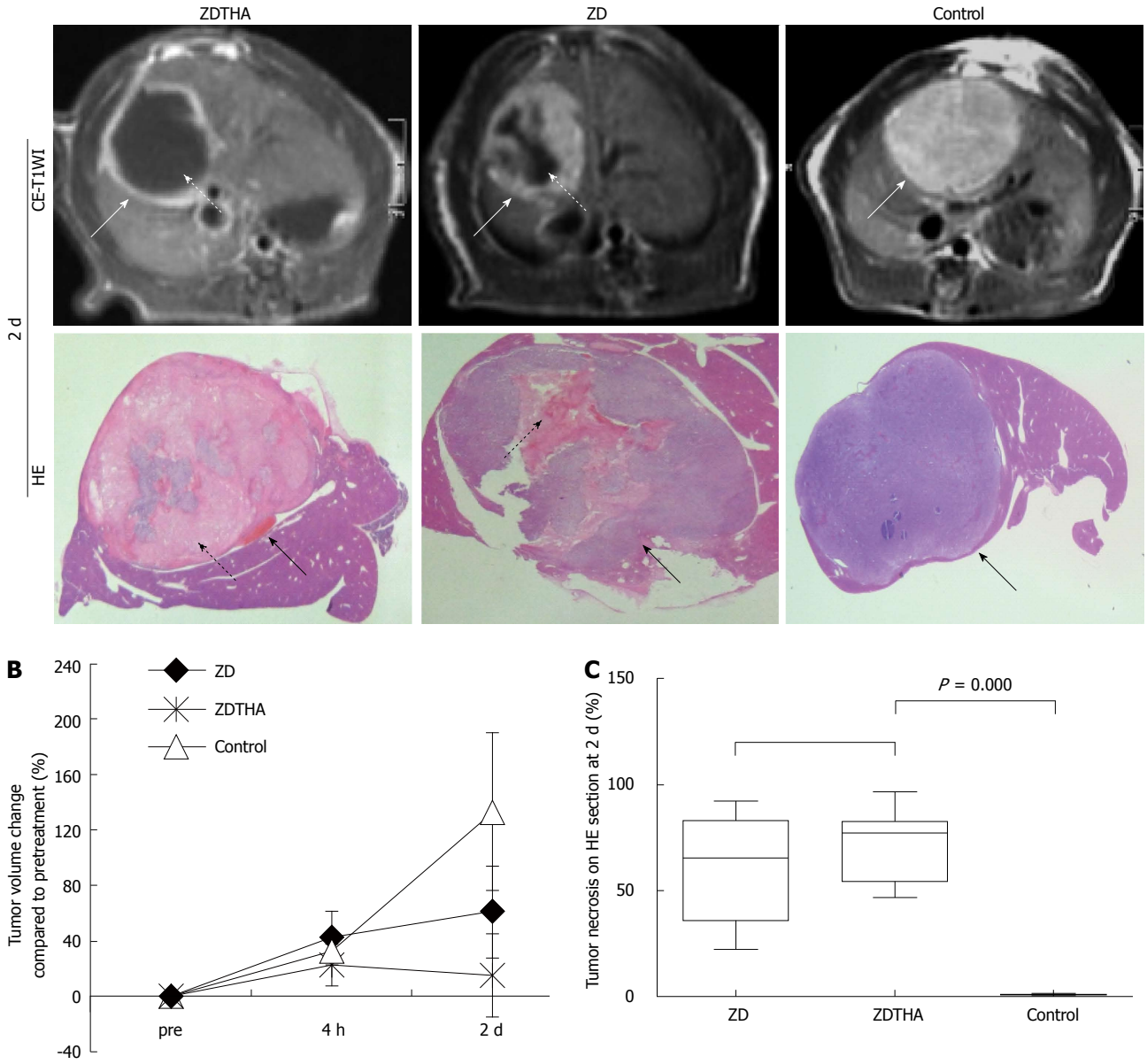

Figure 1 Tumor growth delay. A: Representative axial magnetic resonance images of liver tumors acquired with T2-weighted images (T2WI) [repetition/echo time (TR/TE) = 3860/106 ms], contrast enhanced T1-weighted images (CE-T1WI) (TR/TE = 535/9.2 ms) and HE stained sections. Top row magnetic resonance images: After the combination therapy with ZDTHA, the tumor (solid arrow) in the right liver lobe showed delayed growth with massive central necrotic area (dotted arrow) compared to the control tumor on day 2; Middle row magnetic resonance images: After ZD6126 treatment, the right tumor also showed delayed growth compared to the control tumor on day 2 , however, the tumor necrotic area was reduced (dotted arrow) because the tumor regrew from viable rim; Bottom row magnetic resonance images: In a control animal, the tumor grew remarkably at 2 d; HE sections: The tumor (solid arrow) and central necrotic areas (dotted arrow) in different groups were verified by HE staining; B: The graph indicated that ZDTHA induced a significant tumor volume growth delay during the experiment, compared to both the ZD6126 and control groups ($^{b}P < 0.01$ for both; C: The box plots showed significantly higher percentages of necrotic area (necrosis/tumor) on HE stained sections in both the ZDTHA and ZD6126 groups compared to the control group ($P = 0.000$ for both). No significant difference in necrosis was found between the ZDTHA and ZD6126 groups ($P = 0.09$).

the prostaglandin E pathway[17]. Therefore, the proposed combination therapy with ZD6126 and thalidomide may have some potential applications for solid tumor treatment in clinic.

Second, ADC_{high}, a separate ADC value calculated from high *b* value images, performed significantly better than ADC_{all} for the monitoring of tumor necrosis. In addition to delaying tumor growth, ZDTHA caused tumor necrosis in an additive manner, which was verified by HE staining. Our results showed that although both the ADC_{high} and ADC_{all} of ZDTHA and ZD612 were significantly higher compared to those of the control group on day 2, the entire tumor ADC_{high} of ZDTHA was even higher than that of ZD6126, but the significant difference was not observed for ADC_{all} between ZDTHA and ZD6126. This was due to that ADC_{high} was more sensitive to the diffusion change resulting from the therapeutic necrosis of the tumor on day 2. It has been reported that VDA can cause massive central necrosis 2 d after treatment[18]. Thalidomide can directly induce apoptosis or G1 phase arrest[19]. Consequently, tumor cells treated with ZD6126 and thalidomide underwent increased necrosis compared

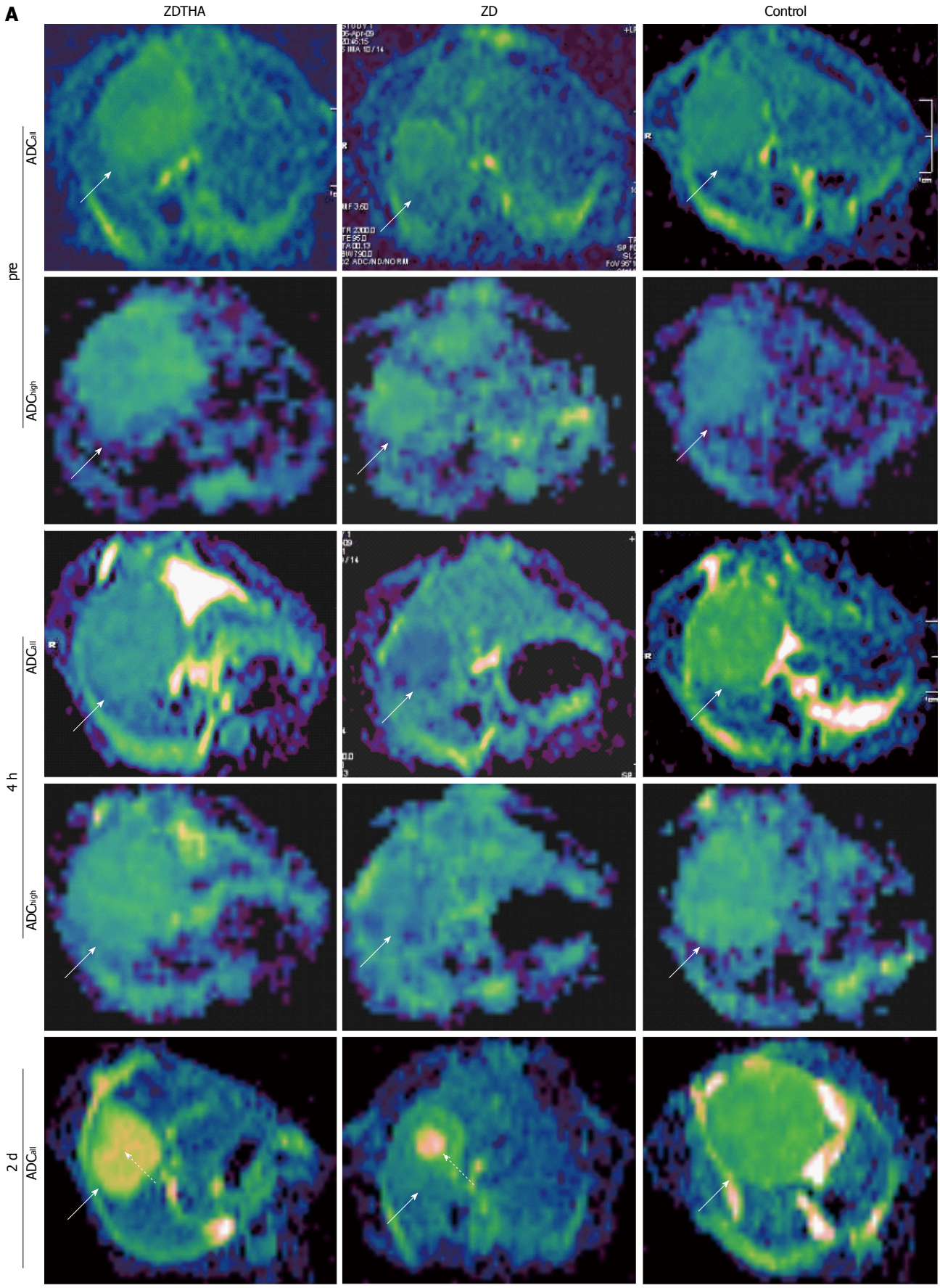
A
ZDTHA
ZD
Control
pre
4 h
2 d
ADCall
ADChigh

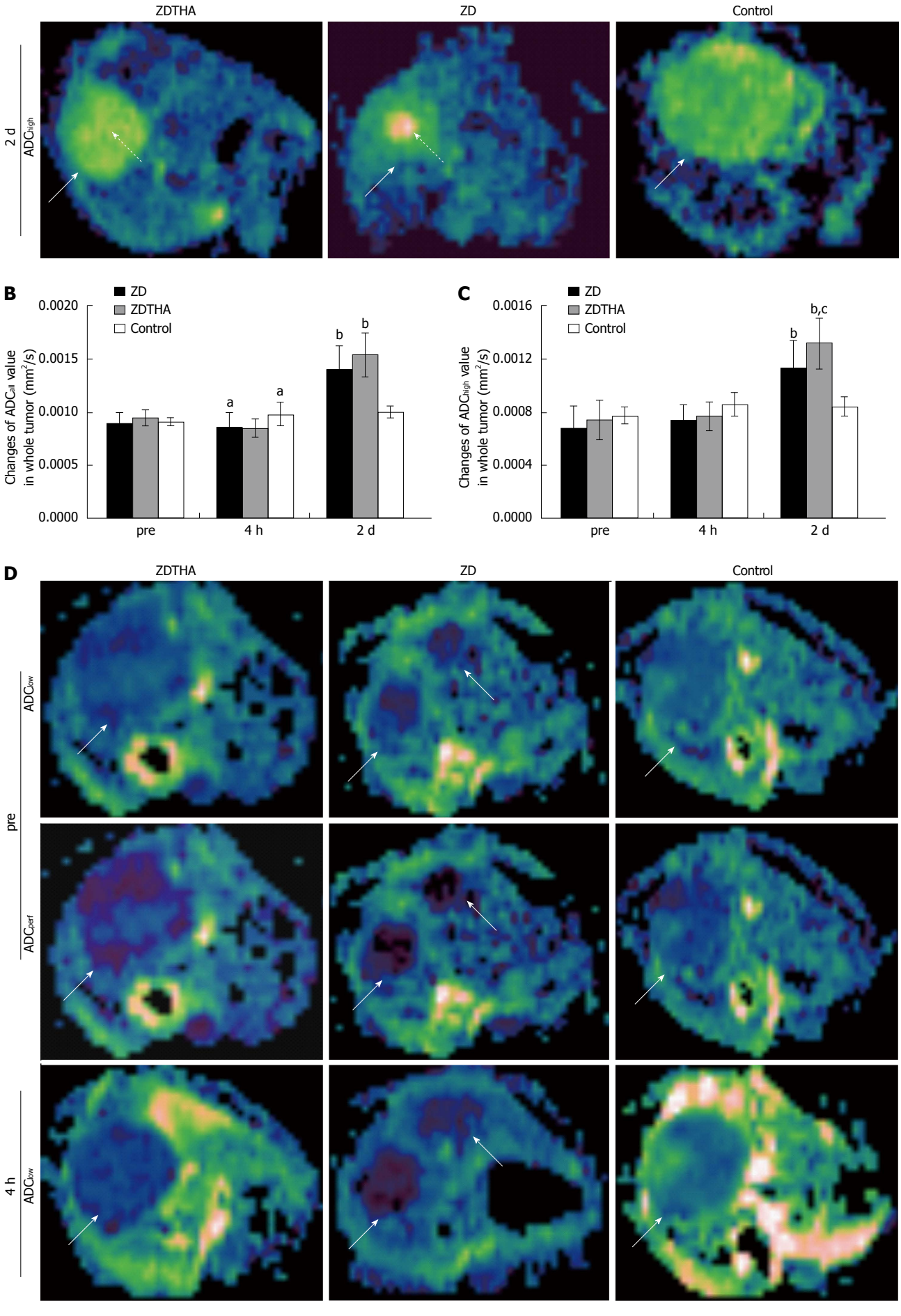
ZDTHA
ZD
Control
2 d
ADChigh
B
ZD
ZDTHA
Control
Changes of ADCall value in whole tumor (mm²/s)
0.0020
0.0015
0.0010
0.0005
0.0000
a
a
b
b
pre
4 h
2 d
C
ZD
ZDTHA
Control
Changes of ADChigh value in whole tumor (mm²/s)
0.0016
0.0012
0.0008
0.0004
0.0000
b
b,c
pre
4 h
2 d
D
ZDTHA
ZD
Control
pre
ADClow
ADCperf
4 h
ADClow

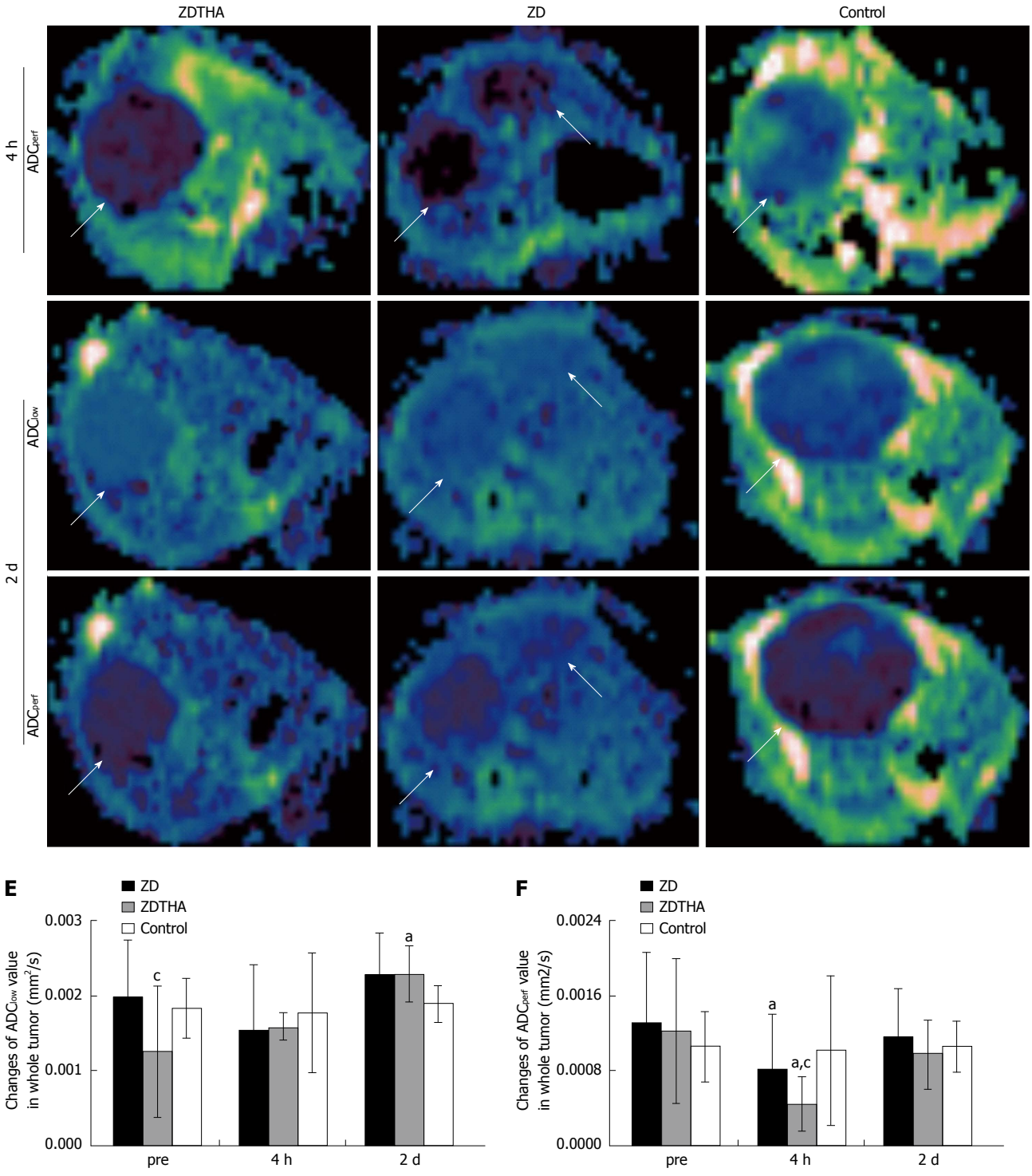

Figure 2 Apparent diffusion coefficient maps for tumors. A: Representative maps of apparent diffusion coefficient $(ADC)_{all}$ and ADC_{high} for liver tumors (solid arrow) in three groups. The area of therapy-induced necrosis (dotted arrow) was significantly larger in the ZDTHA group than those observed in both the ZD6126 and control groups; B: The dynamic change of ADC_{all} during the experiment ($^{a}P < 0.05$, $^{b}P < 0.01$ *vs* control; respectively); C: The dynamic change of ADC_{high} during the experiment. Compared to the ADC_{all}, the increased diffusion due to therapeutic necrosis was better reflected with ADC_{high} in both the ZDTHA and ZD6126 groups on day 2 ($^{b}P < 0.01$ *vs* control; $^{c}P < 0.05$ *vs* ZD6126); D: Representative maps of ADC_{low} and ADC_{perf} for liver tumors (arrow) in the three groups. The signal intensities observed on ADC_{low} maps were always higher than those observed on ADC_{perf} maps at each time point in each group, because ADC_{low} combines both the perfusion and diffusion effects; E: The dynamic change of ADC_{low} during the experiment ($^{a}P < 0.05$ *vs* control; $^{c}P < 0.05$ *vs* ZD6126); F: The dynamic change of ADC_{perf} during the experiment. Compared to the ADC_{low}, the perfusion reduction due to the shutdown of tumor vessels was better reflected with ADC_{perf} in both the ZDTHA and ZD6126 groups at 4 h ($^{a}P < 0.05$ *vs* control). Furthermore, the ADC_{perf} in the ZDTHA group was even lower compared to the ZD6126 group at 4 h ($^{c}P < 0.05$ *vs* ZD6126).

to the single use of ZD6126 at the end of the study; this synergistic effect on necrosis could be better reflected with ADC_{high} as shown in this study.

Third, ADC_{perf}, a separate ADC value calculated as ADC_{low} minus ADC_{high}, can provide valuable perfusion information from DWI data. Although the ADC_{low} was

Table 1 Average apparent diffusion coefficient of entire tumor before and after treatment (mean ± SD)

Group and time	ADC_{all} (× 10^{-3} mm^2/s)	ADC_{high} (× 10^{-3} mm^2/s)	ADC_{low} (× 10^{-3} mm^2/s)	ADC_{perf} (× 10^{-3} mm^2/s)
ZD6126				
Pre	0.90 ± 0.10	0.68 ± 0.16	1.98 ± 0.75	1.30 ± 0.74
4 h	0.86 ± 0.13	0.73 ± 0.12	1.54 ± 0.87	0.81 ± 0.70
2 d	1.40 ± 0.22	1.13 ± 0.21	2.28 ± 0.54	1.15 ± 0.52
ZDTHA				
Pre	0.95 ± 0.08	0.70 ± 0.15	1.25 ± 0.87	1.22 ± 0.77
4 h	0.85 ± 0.08	0.77 ± 0.11	1.21 ± 0.59	0.44 ± 0.50
2 d	1.54 ± 0.21	1.31 ± 0.19	2.28 ± 0.37	0.97 ± 0.36
Control				
Pre	0.91 ± 0.04	0.77 ± 0.07	1.82 ± 0.39	1.06 ± 0.37
4 h	0.98 ± 0.11	0.85 ± 0.09	1.76 ± 0.79	1.01 ± 0.80
2 d	1.00 ± 0.06	0.95 ± 0.08	1.90 ± 0.24	1.06 ± 0.27

Pre: Pretreatment; ZD: ZD6126; ZDTHA: ZD6126 + thalidomide; ADC: Apparent diffusion coefficient; ADC_{all}: Calculated from the entire *b* value setting (*b* = 0, 50, 100, 150, 200, 250, 300, 500, 750, 1000 s/mm^2); ADC_{high}: calculated from the high *b* values (*b* = 500, 750, 1000 s/mm^2); ADC_{low}: Calculated from the low *b* values (*b* = 0, 50, 100 s/mm^2); ADC_{perf}: Calculated from ADC_{low}-ADC_{high}.

calculated from low *b* value images and perfusion sensitive, it was still contaminated with diffusion effects in tissues[15]. Therefore, ADC_{low} was not satisfactory in evaluating the tumor response to treatment as indicated in this study. However, ADC_{perf} was calculated from ADC_{low} by excluding high *b* value effects; it would be more perfusion sensitive. In this study, for instance, strikingly reduced perfusion in response to treatment was detected with ADC_{perf} at 4 h, but not with ADC_{low} for both the ZDTHA and ZD6126 groups compared to the control group. Furthermore, the reduction of ADC_{perf} in ZDTHA was even lower; this indicated a more pronounced decrease in blood perfusion induced by ZDTHA. The ADC_{perf} of ZDTHA still showed a lower level compared to ZD6126 on day 2, although there was no significant difference. This could be explained by the fact that besides the vascular shutdown effect of ZD6126, thalidomide may also induce a transient normalization of tumor vasculature *via* aggressive vascular pruning and improve pericyte coverage on vessels. As a result, tumor perfusion was reduced[20,21]. Our results indicated that ADC_{perf} allowed the early monitoring of therapeutic effects, because it was more sensitive to the microcapillary perfusion and could detect perfusion in response to therapy before the appearance of tumor necrosis without the administration of contrast media.

Similarly, such a significant perfusion reduction at 4 h was also detected with ADC_{all} in both the ZDTHA and ZD6126 groups, however, this was not observed for ADC_{high}, compared to the control group. The reason is that ADC_{all} was derived from 10 *b* values including low and high *b* values; consequently it was affected by both diffusion and perfusion in the tumor. Even though, the perfusion change measured with ADC_{all} was not as striking as that noted with ADC_{perf} due to the influence of diffusion contribution. Despite the delayed growth and the massive central necrotic areas in both the ZDTHA and ZD6126 groups, tumors began to relapse evidenced by the recovery of tumor ADC_{perf} and ADC_{low}, as well as the enhanced rim visualized on CE-T1WI, due to residue viable tumor cells on day 2 after therapy. These results are consistent with previous findings[18,22]. However, ZDTHA demonstrated significantly less tumor relapse than ZD6126, suggesting the benefit of applying the combination therapy.

It remains controversial regarding the option of mono- or biexponential model in extracting diffusion and perfusion information from DWI data. Because each model has its own advantages and drawbacks[15,23]. As a pioneering work in the mid-1986s, Le Bihan *et al*[24,25] proposed the concept of IVIM to address the microscopic movements in image voxel in MRI. In biologic tissue, the motions include the molecular diffusion of water and the microcirculation of blood or capillary perfusion. With the biexponential model of IVIM, the fraction of capillary perfusion can be separated from diffusion. Therefore, there is growing studies using IVIM from DWI data[26-29]. However, the clinical benefit of the biexponential model as compared to the monoexponential model has not been comprehensively established[10,15]. Our study supports that the ADC_{high} values are similar to the diffusion coefficient derived from IVIM model. The separate calculations of ADC_{all}, ADC_{high}, ADC_{low} and ADC_{perf} using a monoexponential fitting algorithm are relatively simple to estimate and are readily available for most users of clinical MR scanners. However, a lack of direct comparison of diffusion parameters derived from mono- and biexponential model may be a limitation of the present study.

In conclusion, we have demonstrated that ZDTHA combination treatment significantly delayed tumor growth due to synergistic effects by inducing cumulative tumor necrosis. The perfusion insensitive ADC_{high} values calculated from high *b* value images performed significantly better than ADC_{all} values for the monitoring of tumor necrosis. The perfusion sensitive ADC_{perf} values derived from ADC_{low} by excluding high *b* value effects could provide valuable perfusion information from DWI data. Therefore, the *in vivo* separate calculations of ADC values derived from monoexponential model are more useful than conventional averaged ADC values in the

successful evaluation of tumor therapeutic effects.

COMMENTS

Background

Diffusion weighted magnetic resonance imaging (DW-MRI), due to its ability to detect molecular water motion at the cellular level, *i.e.*, the measurement of apparent diffusion coefficient (ADC), has become a favorite choice of measures in a variety of oncological studies and tissue viability assessments.

Research frontiers

Technological innovations in recent years have enabled the increasing use of high-quality and quantitative DW-MRI in monitoring tumor treatment. However, it has been realized that the information acquired from conventional calculation of DW-MRI data actually represents the combined effects of tissue microcirculation perfusion and pure tissue diffusivity in each imaging voxel at DW-MRI. This may hinder the appropriate interpretation of the DW-MRI data. Therefore, there is growing interest in applying more sophisticated approaches, such as separate ADC (calculating different ADC values based on various combinations of *b* values with a monoexponential fitting algorithm) and intravoxel incoherent motion, to differentiate the fraction of microcirculation perfusion from pure diffusivity within the DW-MRI data.

Innovations and breakthroughs

The combination therapy with ZD6126 and thalidomide significantly delayed liver tumor growth due to synergistic effects by inducing cumulative tumor necrosis in rodents. The ADC_{high} performed significantly better than ADC_{all} for the monitoring of tumor necrosis on day 2. The ADC_{perf} could better reflect the reduction of blood flow due to the vessel shutdown induced by ZD6126, compared to the ADC_{low}. The ADC_{perf} could provide valuable perfusion information from diffusion weighted MRI data.

Applications

The separate calculation of ADC is more useful than conventional averaged ADC in evaluating the efficacy of combination therapy with ZD6126 and thalidomide for solid tumors.

Terminology

DW-MRI is an *in vivo* imaging technique to detect molecular water motion at the cellular level by using the ADC parameter. Separate ADC measurement is to calculate the different ADC values based on various combinations of *b* values with a monoexponential fitting algorithm.

Peer review

The authors present ADC is more useful than conventional averaged ADC in evaluating the efficacy of combination therapy with ZD6126 and thalidomide for solid tumors. It would be of interest to perform the same study in a vascular tumor such as infantile hemangioma or a malignant vascular tumor such as angiosarcoma or hemangiopericytoma.

REFERENCES

1 **Dark GG**, Hill SA, Prise VE, Tozer GM, Pettit GR, Chaplin DJ. Combretastatin A-4, an agent that displays potent and selective toxicity toward tumor vasculature. *Cancer Res* 1997; **57**: 1829-1834 [PMID: 9157969]

2 **Tozer GM**, Kanthou C, Baguley BC. Disrupting tumour blood vessels. *Nat Rev Cancer* 2005; **5**: 423-435 [PMID: 15928673 DOI: 10.1038/nrc1628]

3 **Kanthou C**, Tozer GM. Microtubule depolymerizing vascular disrupting agents: novel therapeutic agents for oncology and other pathologies. *Int J Exp Pathol* 2009; **90**: 284-294 [PMID: 19563611 DOI: 10.1111/j.1365-2613.2009.00651.x]

4 **Siemann DW**. The unique characteristics of tumor vasculature and preclinical evidence for its selective disruption by Tumor-Vascular Disrupting Agents. *Cancer Treat Rev* 2011; **37**: 63-74 [PMID: 20570444 DOI: 10.1016/j.ctrv.2010.05.001]

5 **Padhani AR**, Miles KA. Multiparametric imaging of tumor response to therapy. *Radiology* 2010; **256**: 348-364 [PMID: 20656830 DOI: 10.1148/radiol.10091760]

6 **Thoeny HC**, De Keyzer F, Chen F, Vandecaveye V, Verbeken EK, Ahmed B, Sun X, Ni Y, Bosmans H, Hermans R, van Oosterom A, Marchal G, Landuyt W. Diffusion-weighted magnetic resonance imaging allows noninvasive in vivo monitoring of the effects of combretastatin a-4 phosphate after repeated administration. *Neoplasia* 2005; **7**: 779-787 [PMID: 16207480 DOI: 10.1593/neo.04748]

7 **Thoeny HC**, De Keyzer F, Vandecaveye V, Chen F, Sun X, Bosmans H, Hermans R, Verbeken EK, Boesch C, Marchal G, Landuyt W, Ni Y. Effect of vascular targeting agent in rat tumor model: dynamic contrast-enhanced versus diffusion-weighted MR imaging. *Radiology* 2005; **237**: 492-499 [PMID: 16192323 DOI: 10.1148/radiol.2372041638]

8 **Thoeny HC**, De Keyzer F, Chen F, Ni Y, Landuyt W, Verbeken EK, Bosmans H, Marchal G, Hermans R. Diffusion-weighted MR imaging in monitoring the effect of a vascular targeting agent on rhabdomyosarcoma in rats. *Radiology* 2005; **234**: 756-764 [PMID: 15734932 DOI: 10.1148/radiol.2343031721]

9 **Sun X**, Wang H, Chen F, De Keyzer F, Yu J, Jiang Y, Feng Y, Li J, Marchal G, Ni Y. Diffusion-weighted MRI of hepatic tumor in rats: comparison between in vivo and postmortem imaging acquisitions. *J Magn Reson Imaging* 2009; **29**: 621-628 [PMID: 19243058 DOI: 10.1002/jmri.21675]

10 **Chandarana H**, Lee VS, Hecht E, Taouli B, Sigmund EE. Comparison of biexponential and monoexponential model of diffusion weighted imaging in evaluation of renal lesions: preliminary experience. *Invest Radiol* 2011; **46**: 285-291 [PMID: 21102345]

11 **Yamada I**, Aung W, Himeno Y, Nakagawa T, Shibuya H. Diffusion coefficients in abdominal organs and hepatic lesions: evaluation with intravoxel incoherent motion echo-planar MR imaging. *Radiology* 1999; **210**: 617-623 [PMID: 10207458]

12 **Kivivuori SM**, Riikonen P, Valanne L, Lönnqvist T, Saarinen-Pihkala UM. Antiangiogenic combination therapy after local radiotherapy with topotecan radiosensitizer improved quality of life for children with inoperable brainstem gliomas. *Acta Paediatr* 2011; **100**: 134-138 [PMID: 20712831 DOI: 10.1111/j.1651-2227.2010.01961.x]

13 **Chen F**, Sun X, De Keyzer F, Yu J, Peeters R, Coudyzer W, Vandecaveye V, Landuyt W, Bosmans H, Van Hecke P, Marchal G, Ni Y. Liver tumor model with implanted rhabdomyosarcoma in rats: MR imaging, microangiography, and histopathologic analysis. *Radiology* 2006; **239**: 554-562 [PMID: 16543589 DOI: 10.1148/radiol.2392050277]

14 **Chen F**, De Keyzer F, Wang H, Vandecaveye V, Landuyt W, Bosmans H, Hermans R, Marchal G, Ni Y. Diffusion weighted imaging in small rodents using clinical MRI scanners. *Methods* 2007; **43**: 12-20 [PMID: 17720559 DOI: 10.1016/j.ymeth.2007.03.007]

15 **Koh DM**, Collins DJ, Orton MR. Intravoxel incoherent motion in body diffusion-weighted MRI: reality and challenges. *AJR Am J Roentgenol* 2011; **196**: 1351-1361 [PMID: 21606299 DOI: 10.2214/AJR.10.5515]

16 **van Heeckeren WJ**, Sanborn SL, Narayan A, Cooney MM, McCrae KR, Schmaier AH, Remick SC. Complications from vascular disrupting agents and angiogenesis inhibitors: aberrant control of hemostasis and thrombosis. *Curr Opin Hematol* 2007; **14**: 468-480 [PMID: 17934353 DOI: 10.1097/MOH.0b013e3282a6457f]

17 **Reck M**, Gatzemeier U. Targeted therapies: Thalidomide in lung cancer therapy-what have we learned? *Nat Rev Clin Oncol* 2010; **7**: 134-135 [PMID: 20190796 DOI: 10.1038/nrclinonc.2010.11]

18 **Wang H**, Sun X, Chen F, De Keyzer F, Yu J, Landuyt W, Vandecaveye V, Peeters R, Bosmans H, Hermans R, Marchal G, Ni Y. Treatment of rodent liver tumor with combretastatin a4 phosphate: noninvasive therapeutic evaluation using multiparametric magnetic resonance imaging in correlation with microangiography and histology. *Invest Radiol* 2009; **44**: 44-53 [PMID: 19034028 DOI: 10.1097/

RLI.0b013e31818e5ace]
19 **Figg WD**, Li H, Sissung T, Retter A, Wu S, Gulley JL, Arlen P, Wright JJ, Parnes H, Fedenko K, Latham L, Steinberg SM, Jones E, Chen C, Dahut W. Pre-clinical and clinical evaluation of estramustine, docetaxel and thalidomide combination in androgen-independent prostate cancer. *BJU Int* 2007; **99**: 1047-1055 [PMID: 17437439 DOI: 10.1111/j.1464-410X.2007.06763.x]
20 **Chen F**, Feng Y, Zheng K, De Keyzer F, Li J, Feng Y, Cona MM, Wang H, Jiang Y, Yu J, Marchal G, Verfaillie C, De Geest B, Oyen R, Ni Y. Enhanced antitumor efficacy of a vascular disrupting agent combined with an antiangiogenic in a rat liver tumor model evaluated by multiparametric MRI. *PLoS One* 2012; **7**: e41140 [PMID: 22815943 DOI: 10.1371/journal.pone.0041140]
21 **Stewart EE**, Sun H, Chen X, Schafer PH, Chen Y, Garcia BM, Lee TY. Effect of an angiogenesis inhibitor on hepatic tumor perfusion and the implications for adjuvant cytotoxic therapy. *Radiology* 2012; **264**: 68-77 [PMID: 22627603 DOI: 10.1148/radiol.12110674]
22 **Wang H**, Li J, Chen F, De Keyzer F, Yu J, Feng Y, Nuyts J, Marchal G, Ni Y. Morphological, functional and metabolic imaging biomarkers: assessment of vascular-disrupting effect on rodent liver tumours. *Eur Radiol* 2010; **20**: 2013-2026 [PMID: 20182730 DOI: 10.1007/s00330-010-1743-5]
23 **Rheinheimer S**, Stieltjes B, Schneider F, Simon D, Pahernik S, Kauczor HU, Hallscheidt P. Investigation of renal lesions by diffusion-weighted magnetic resonance imaging applying intravoxel incoherent motion-derived parameters--initial experience. *Eur J Radiol* 2012; **81**: e310-e316 [PMID: 22104090 DOI: 10.1016/j.ejrad.2011.10.016]
24 **Le Bihan D**, Breton E, Lallemand D, Grenier P, Cabanis E, Laval-Jeantet M. MR imaging of intravoxel incoherent motions: application to diffusion and perfusion in neurologic disorders. *Radiology* 1986; **161**: 401-407 [PMID: 3763909]
25 **Le Bihan D**, Breton E, Lallemand D, Aubin ML, Vignaud J, Laval-Jeantet M. Separation of diffusion and perfusion in intravoxel incoherent motion MR imaging. *Radiology* 1988; **168**: 497-505 [PMID: 3393671]
26 **Le Bihan D**. Intravoxel incoherent motion perfusion MR imaging: a wake-up call. *Radiology* 2008; **249**: 748-752 [PMID: 19011179 DOI: 10.1148/radiol.2493081301]
27 **Takahara T**, Kwee TC. Low b-value diffusion-weighted imaging: emerging applications in the body. *J Magn Reson Imaging* 2012; **35**: 1266-1273 [PMID: 22359279 DOI: 10.1002/jmri.22857]
28 **Guiu B**, Petit JM, Capitan V, Aho S, Masson D, Lefevre PH, Favelier S, Loffroy R, Vergès B, Hillon P, Krausé D, Cercueil JP. Intravoxel incoherent motion diffusion-weighted imaging in nonalcoholic fatty liver disease: a 3.0-T MR study. *Radiology* 2012; **265**: 96-103 [PMID: 22843768 DOI: 10.1148/radiol.12112478]
29 **Pang Y**, Turkbey B, Bernardo M, Kruecker J, Kadoury S, Merino MJ, Wood BJ, Pinto PA, Choyke PL. Intravoxel incoherent motion MR imaging for prostate cancer: an evaluation of perfusion fraction and diffusion coefficient derived from different b-value combinations. *Magn Reson Med* 2013; **69**: 553-562 [PMID: 22488794]

P- Reviewers: Casal Moura M, Fernandez-Pineda I
S- Editor: Zhai HH **L- Editor**: Wang TQ **E- Editor**: Ma S

百世登

Baishideng®

Published by **Baishideng Publishing Group Co., Limited**
Flat C, 23/F., Lucky Plaza,
315-321 Lockhart Road, Wan Chai, Hong Kong, China
Fax: +852-65557188
Telephone: +852-31779906
E-mail: bpgoffice@wjgnet.com
http://www.wjgnet.com

ISSN 1007-9327